Electron emission and structural characterization of a rope of single-walled carbon nanotubes

D. Lovall

Department of Physics, Purdue University, West Lafayette, Indiana 47907

M. Buss

School of Chemical Engineering, Purdue University, West Lafayette, Indiana 47907

E. Graugnard

Department of Physics, Purdue University, West Lafayette, Indiana 47907

R. P. Andres

School of Chemical Engineering, Purdue University, West Lafayette, Indiana 47907

R. Reifenberger

Department of Physics, Purdue University, West Lafayette, Indiana 47907

The electron emission and structural properties of an isolated ''rope'' comprised of $\sim$70 individual single-walled nanotubes (SWNT's) were investigated by measuring the field-emission energy distributions and by using field-ion microscopy (FIM). Field-emission energy distributions, obtained under ultrahigh-vacuum conditions, revealed that the emitting nanotube has a large density of states near the Fermi energy, with an energy distribution of emitted electrons close to that predicted by the free-electron theory. Two small features located on the trailing edge of the energy distributions are attributed to localized features in the density of states of a SWNT. FIM studies were also performed on the same rope in an attempt to provide structural information about the emitting nanotube. Initial FIM micrographs showed an uneven distribution of atoms. Eventually, rings of atoms were imaged. The atom placement around an individual ring structure is analyzed and found to be consistent with that expected from a single (19,13) SWNT.

I. INTRODUCTION

Much work has been done toward an understanding of the structural and electronic properties of carbon nanotubes. Many calculations of the electronic structure of single-walled nanotubes (SWNT's) have been reported.[1–4] SWNT's of the armchair (n,n) variety are expected to be metallic; nanotubes of the zigzag $(n,0)$ family can be either metallic or semiconducting; and nanotubes with an inherent (n,m) helicity are expected to be either semiconducting or metallic, depending on the exact values of n and m. Calculations illustrating how the density of states (DOS) varies near the capped end of a nanotube have also been reported.[5–7]

Nanotubes can be imaged in the transmission electron microscope (TEM) relatively easily which has provided an understanding of the structural properties and the growth mechanisms involved in nanotube formation.[3,8–10] Scanning tunneling microscope (STM) studies have also yielded valuable structural information and insight into the correlation between the atomic structure and the local electronic properties of a nanotube.[11–16] The STM studies, combined with experimental studies of the temperature and magnetic-field dependence of the electrical resistivity, have provided evidence consistent with a one-dimensional conductor.[1,17,18]

Also, many studies of field emission from carbon fiber tips[19–21] and unoriented arrays (i.e., ''films'') of carbon nanotubes have appeared.[18,20,22–25] Recently, studies of field emission from single multiwalled nanotubes (MWNT's)[10,26,27] and SWNT's[28] have been published. These studies are in part motivated by a long-term interest in new, stable electron emitters for a variety of electronic devices. It is known that carbon fibers are capable of maintaining large, stable emission currents ($\geqslant 2\ \mu$A) for long periods of time.[21] In contrast, it has been reported that carbon nanotubes burn out at emission currents greater than $\sim$1 μA.[26]

In spite of this effort, little is known about the energy distribution of electrons emitted from carbon nanotubes.[25] Information such as the angular spread and the dispersion in energy of the emitted electrons provides important information that might be useful in assessing the potential of carbon nanotubes for a variety of future applications. More work is needed to better understand and characterize these important electron emission properties of carbon nanotubes.

In what follows we describe experiments that attempt to answer some of the important questions regarding the current stability and the electrotonic and structural properties of carbon nanotubes. We have measured the energy distribution of emitted electrons from a rope of SWNT's and attempted to characterize the structural properties of the same rope by measuring the position of carbon atoms using a field-ion microscope (FIM). To ensure a cleaner environment than used in prior studies,[18,22,26] measurements have been performed at operating pressures around 10^{-9} Torr.

II. EXPERIMENTAL CONSIDERATIONS

A. Sample preparation

The samples used in this study were obtained from a boule of SWNT's which were synthesized at Rice University. Based on size and energy considerations, the SWNT

boule is expected to be comprised to be comprised of ropes of various diameters which are in turn comprised of single nanotubes.[29,30] Based on Raman-selective data,[30] the individual (n,m) nanotubes studied here are thought to be structurally characterized by indices bounded roughly by the constraints $6 < n < 15$ and $6 < m < 12$.

A SWNT rope was mounted on a Pt field-emission tip using a procedure similar to that described by Dai *et al.*[31] The Pt tip was etched in a saturated $CaCl_2$ solution to an end radius of ~ 100 nm. The rope was attached by using an inverted optical microscopy (Nikon Epiphot 200) equipped with a $50X/0.55$ objective to observe the process in darkfield at $750X$ magnification. Two micromanipulators (Newport M-$460A$-XYZ) were bolted onto the microscope stage and used to attach the SWNT rope to the Pt field emission tip.

The process involved the transfer of a small amount of conducting adhesive from an scanning electron microscope tape to the Pt tip by touching the tip to a clean portion of tape and carefully removing it. A SWNT rope was then stuck to the coated tip by bringing the tip into proximity with the SWNT boule. Contact to a SWNT rope was realized when movement of the Pt tip produced movement of a visible part of the boule. At this moment, the Pt tip was connected to the visible boule through an invisible SWNT rope. A small voltage (~ 10 V) was then applied between the tip and boule to break the rope loose from the boule. Often a visible emission of light is observed during this break-off procedure, implying the presence of a localized, intense electrical arc. It should be noted that the spark removal of the rope from the boule breaks the rope somewhere along its length. It is therefore likely that the tubes in the rope remain open and do not close, as has been reported elsewhere.[32,33]

After mounting, the SWNT rope was examined using a TEM (JEOL 2000 FX). The SWNT rope used for the studies reported below is shown in Fig. 1. From this micrograph, the diameter of the SWNT rope is determined to be 17.0 ± 1.0 nm. Choosing a representative diameter of a typical nanotube to be roughly ~ 1.4 nm, and since each nanotube is separated from another by ~ 0.3 nm, we estimate that ~ 70 individual nanotubes are contained in this rope. After the TEM study was complete, the Pt tip/SWNT rope assembly was inserted into our field-emission/field-ion microscope apparatus.

B. Field emission and field-ion microscopy

The field-emission and field-ion experiments were performed in a homebuilt UHV chamber specifically designed for studies of electron emission from nanometer-size structures. It features an XYZ-$\Theta\Phi$ manipulator with five degrees of freedom, on which the SWNT tips are placed. Tips are mounted on small metal tabs which allow the tip/nanotube unit to be transferred from the TEM to the field emission microscope/field-ion microscope (FEM/FIM) chamber without disturbing the sample.

Because of the atomic resolution capability of a FIM this technique was employed in an attempt to learn more about the atomic structure of the emitting nanotube. Prior FIM of carbon structures has been performed with mixed results. Tsong published FIM images of graphite tips using He as an imaging gas,[34] where the images showed the basal planes of
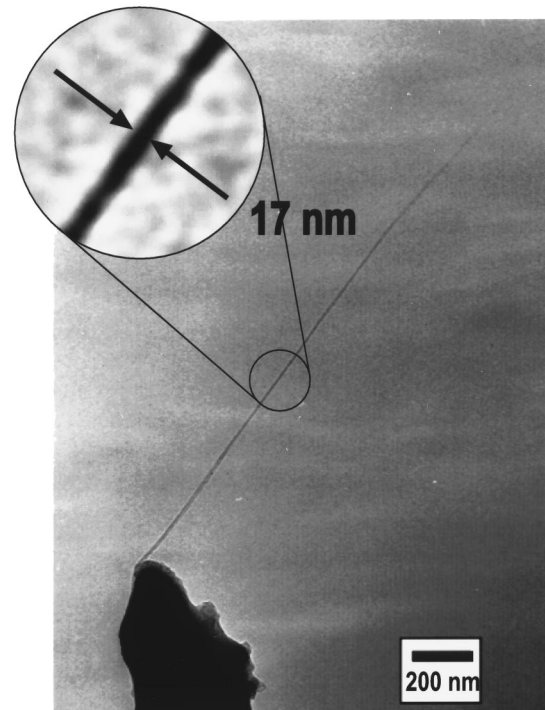

FIG. 1. A TEM micrograph of a single-walled carbon nanotube (SWNT) rope mounted on a Pt field emitter. The micrograph shows that the SWNT is oriented at an angle of about 45° from the axis of the Pt support. The inset shows a section under higher magnification, and permits a determination of the rope's diameter. The end form of the rope could not be clearly imaged due to vibrations.

graphite but were not atomically resolved. More and Joag[19] reported He ion imaging of a carbon fiber tip which suggests a graphite structure.

The FIM itself is equipped with a small fluorescent screen and a multichannel plate with an integral fluorescent screen, either of which can be used to image the SWNT rope. The tip to screen distance R is ~ 13 cm. Since the FIM is essentially a point projection microscope, it has a magnification given by[35]

$$M \simeq \frac{R}{\alpha r_{\text{tip}}}, \tag{1}$$

where r_{tip} is the radius of the emitting object. The field lines which the ions follow are compressed by the dimensionless factor α due to the presence of the tip shank. This compression can be calculated if the ion paths are known, but it is usually much simpler to estimate α directly from an FIM micrograph. A value of 1.5 is typical for conventional metallic emission tips.[35]

In order to interpret any observed FIM image, it is useful to perform a thin-shell simulation based on an assumed atomic structure. The thin-shell algorithm employed here assumes that the FIM image results from the ionization of an imaging gas over the atoms terminating the nanotube. Thus, a bright spot represents a projection of a C atom from the nanotube onto a nearly fluorescent screen. The relative position of the ionized gas atoms on the screen were determined by projecting the ion trajectories from a point $2r_{\text{tip}}$ behind the end of the nanotube and rope, where r_{tip} is some effective

radius of the nanotube. In our simulations, the image spots are broadened by a Gaussian to approximate the finite resolution of the FIM operating at 100 K. This technique was used previously to successfully interpret field-ion images from nanometer-size Au clusters.[36]

The FIM chamber is also equipped with an Omicron electron energy analyzer built on a cylindrical sector analyzer design having an entrance probe hole of 1 cm in diameter. The performance of the analyzer was tested by collecting and analyzing energy distributions from well-known field emitters like W(110) in separate experiments. This apparatus gives us to unique ability to study both the structural and electronic properties of the same nanotube.

III. RESULTS

A. Field emission from a SWNT rope

A priori, it is difficult to know whether the electron emission from a SWNT rope is governed by electron emission from all nanotubes comprising the rope of from a single nanotube that protrudes slightly further from the rope than all the other nanotubes. We consider it likely that a single nanotube does protrude from the rope and will experience an enhanced electric field, in much the same way that the electric field is enhanced over a small nanometer-size protrusion located on a substrate having a larger radius of curvature.[37] This enhancement depends on the distance that an individual nanotube protrudes from the end of the rope and can be estimated if the diameters of the rope and the protruding nanotube are known. Estimates based on the field enhancement for whiskers[38] indicate that a factor of order 2 may result. This will insure that the electron current from the rope is dominated by the protruding nanotube. We also assume that the nanotube does not posses an endcap because of the spark removal of the rope from the boule (see discussion above). We analyze the data with these two assumptions in mind.

Initial attempts at imaging SWNT's using field emission were frustrated by the inherent weakness of the resulting images on a fluorescent screen. Because the ropes are so sharp, they field emit at relatively low voltages (compared to W emitters), producing an electron beam with insufficient energy to excite the phosphor in our viewing screen. This problem was solved by using a multichannel plate equipped with an integral phosphor screen. The field-emission patterns were observed to be stable and continuous as shown by a contour plot of the image intensity taken from the field-emission pattern produced by our SWNT rope (see Fig. 2). No striations or banding in the field-emission pattern, an attribute of caped nanotubes, were observed here.[25,39]

A study of the field-emission pattern produced by an emitting object is useful for a number of reasons. First and foremost, the pattern reveals any relative anisotropy in the work function and/or geometry of the emitting object. In the case of conventional field emission tips, the underlying crystallographic symmetry of the emitting tip is often revealed. For these reasons, the hint of a threefold symmetry evident in the emission pattern in Fig. 2 is interesting.

A measure of the angular distribution of the emitted electrons is useful for a number of practical reasons related to electron emission in both electron microscopes and for nano-
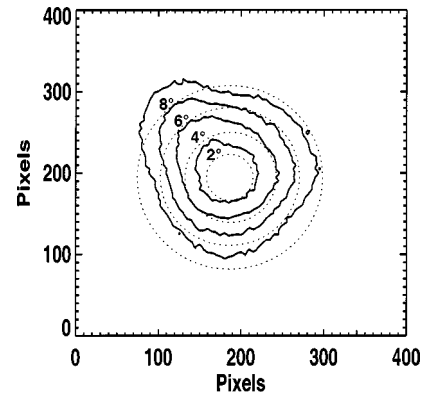

FIG. 2. A plot of the contours of constant intensity taken from the recorded image of the field-emission pattern observed in this study. The apparent threefold symmetry in this image is either related to a slight distortion in the geometry of the SWNT rope or to an anisotropy in the work function of the emitting nanotube. The dotted circles represent the half-angle of electron emission, and are useful to estimate the angular width of the emitted electron beam.

lithography employing STM techniques. The half-angle width of the emitted electron beam measured here can be inferred from the dotted fiducial circles in Fig. 2. A conclusion from this study is that the entire electron beam is essentially confined to a cone having an angular span of roughly $\pm 7°$.

To verify that the electron emission from the SWNT rope was governed by a field-emission process, a Fowler-Nordheim analysis was performed, even though a traditional Fowler-Nordheim theory may not be strictly applicable because of the small radius of the SWNT rope. According to Fowler and Nordheim, the current density J is related to the applied field F by[40]

$$J = AF^2 e^{-(B\phi^{3/2}/F)}. \qquad (2)$$

Here A and B are parameters weakly dependent on the applied electric field and ϕ is the work function of the emitting surface. A proportionality constant β relates the applied voltage V to the resulting electric field F by $F = \beta V$. Ultimately, β can be related to the tip geometry (r_{tip}) and a field compression factor k (which is typically equal to 5 for etched metallic tips), using

$$\beta = \frac{1}{k r_{tip}}. \qquad (3)$$

It follows that a Fowler-Nordheim plot of the emitted current vs. applied voltage [i.e. a plot of $\ln(I/V^2)$ vs $1/V$] is linear if the electron current is governed by field emission.

A representative Fowler-Nordheim plot of data from the SWNT rope is shown in Fig. 3. In most cases, a known work function is assumed and then a value of β is inferred from such data. Here we choose to estimate the work function from the data by roughly estimating β from Eq. (3). By assuming a radius of $r_{tip} = 8.5 \pm 0.5$ nm, as measured from the TEM shown in Fig. 1, we estimate that $\beta = (2.4 \pm 0.4) \times 10^5$ cm^{-1}. Using this value and the measured slope of the Fowler-Nordheim plot in Fig. 3, the work function of the SWNT emitter can be estimated [using Eq. (2)] to equal 5.1
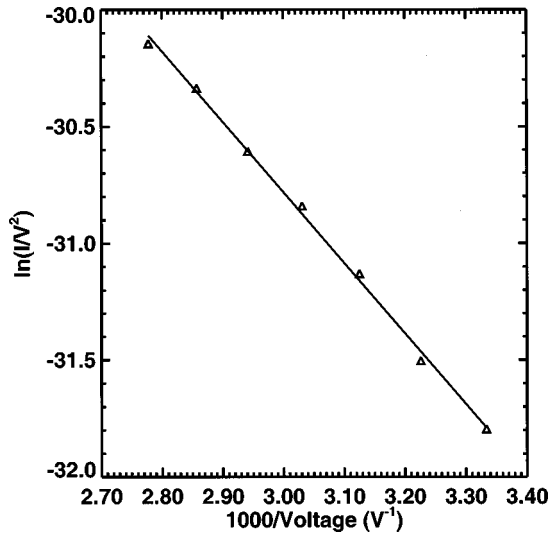
FIG. 3. A Fowler-Nordheim plot from the SWNT rope. The field constant β is estimated to be 2.4×10^5 cm^{-1}. There is a work function of $\phi = 5.1$ eV for the emitting SWNT results.

eV. This value is consistent with expectations for the known work functions of many refractory metals.[41]

B. Total-energy distribution of emitted electrons from a SWNT rope

A measurement of the total-energy distribution (TED) of electrons field emitted from an object in the presence of an applied electric field F can give insights into the underlying electronic structure of the emitting tip.[42,43] The relevant factors contributing to the shape of the total energy distribution from a SWNT are summarized in Fig. 4. As indicated schematically in this figure, the overall shape of the emitted electron distribution is determined by the exponential decrease in tunneling probability below E_F due to the barrier widening. In addition, small features in the electron distribution should be visible at energies $E_1, E_2, \ldots$, where singularities occur in the DOS.

For a metal, the current density j is expected to depend on the energy relative to the Fermi energy $\epsilon = E - E_F$ as[43]

$$j(\epsilon) = \frac{J_0}{d} e^{\epsilon/d} f(\epsilon), \qquad (4)$$

with $f(\epsilon)$ being the Fermi-Dirac distribution function. The factor d is related to the applied electric field F and work function ϕ, and is given by

$$\frac{1}{d} = 2 \left[\frac{2m}{\hbar^2} \right]^{1/2} \frac{\sqrt{\phi}}{eF} t(y) \qquad (5)$$

where $t(y)$ (with $y = \sqrt{e^3 F/\phi}$) is a tabulated dimensionless constant[43] that takes into account the surface barrier lowering by the applied electric field (see Fig. 4).

A representative TED obtained at 300 K with the SWNT rope shown in Fig. 1 biased -250 V relative to ground in a vacuum of $\sim 5 \times 10^{-9}$ Torr is plotted in Fig. 5. For further analysis, we find it convenient to plot the TED as ln (counts) vs energy with the zero of energy set to equal the Fermi energy of the emitter. Data were taken on this emitter over a
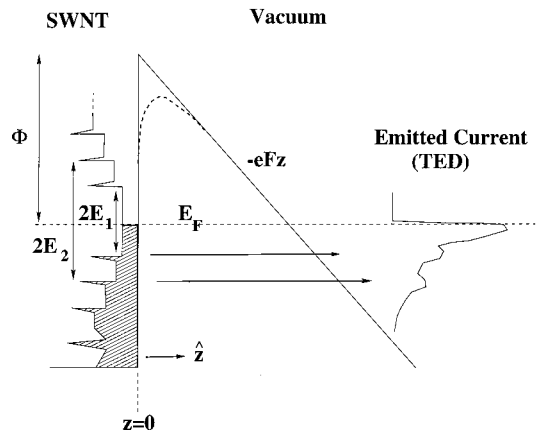

FIG. 4. A schematic of the field-emission process. The potential barrier at the vacuum interface is deformed by the application of a large electric field F. The simplest model for this deformation results in a barrier having a triangular shape ($-eFz$). The barrier is further rounded when image-charge effects are considered. The figure also qualitatively illustrates the contribution that the electronic states of a metallic SWNT might make to the emitted current. The emitted distribution of electrons is referred to as the total-energy distribution (TED). The shaded region illustrates those states below the Fermi energy (E_F) which are occupied and contribute to the field-emission current. Although all singularities below E_F contribute to the field-emitted current, a degradation of the signal-to-noise ratio makes it difficult to observe any features located more than ~ 1.5 eV below E_F. For this reason, only those features located at energies E_1 and E_2 are considered.

period of eight days. The emitted current was stable and the shape of the energy distribution did not change appreciably during the period of time the emitter was studied.

In general, the TED displays an asymmetry consistent with Eq. (4), with a sharp leading edge determined by a convolution of the Fermi-Dirac function with the energy resolution of the analyzer and a significantly broader trailing edge determined largely by the exponential decrease with energy of the transmission function of electrons through the surface potential barrier. Fits to the overall shape of the experimental TED must include both the energy distribution given by Eq. (4) and a convolution with a Gaussian function,[44]

$$\Theta = \frac{1}{\sigma \sqrt{2\pi}} \theta^{-[E-E_0]^2/2\sigma^2} \qquad (6)$$

to represent the energy resolution of the energy analyzer. The full width at half maximum (FWHM) of the analyzer, Γ, is given by $\Gamma = 2.356\sigma$.

Equations (4)–(6) were used to fit the experimental energy distribution. To optimize the fits to the leading edge (i.e., $E > E_F$) of the experimental TED, we convoluted the theoretical calculation with a Gaussian having $\Gamma = 0.20$ eV. A work function $\phi = 5.1$ eV (obtained from the Fowler-Nordheim analysis) was also used in the theoretical fit. Since the value of the electric field controls the width of the energy distribution, fits for three values of F are plotted in Fig. 5. Using the value of β obtained from Fig. 3, one might anticipate a value of $F = 6 \times 10^7$ V/cm to give the best fit. This expectation is indeed met by the fits.
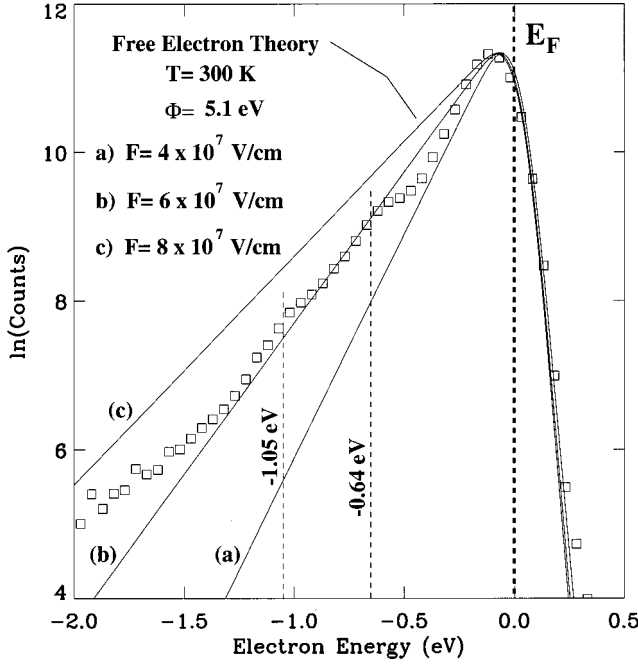
FIG. 5. The natural logarithm of detected counts vs energy for an electrons field emitted from a SWNT rope. The data were taken at $T = 300$ K. The solid lines show the predictions of a free-electron theory for three different values of the electric field F. The calculations are normalized to the peak value in the measured energy distribution. A Gaussian has been convoluted with the free-electron calculation to approximate the resolution of the energy analyzer, which is estimated to be 0.20-eV FWHM. The position of the Fermi energy (E_F) and the two features in the TED (-0.64 and -1.05 eV) are marked by dotted lines.

The overall agreement between theory and data provides evidence for a significant DOS near E_F. We attribute these states to the dangling-bond states that are present at E_F for open nanotubes,[7] suggesting that perhaps greater emission currents can be obtained from open rather than capped tubes. We find that the full width at half maximum of the measured energy distribution depends slightly on the energy analyzer settings, but is roughly 0.35 ± 0.05 eV. This value includes the (estimated) 0.20-eV FWHM resolution of the energy analyzer deduced from the fits in Fig. 5. Interestingly, two small features are observed on the trailing edge of the energy distribution as marked by the two dotted lines in Fig. 5. The location of these features are (0.64 ± 0.05) eV and (1.05 ± 0.05) eV below E_F.

It is useful to attempt a comparison with published DOS calculations to see if the features observed here are roughly consistent with theoretical expectations. This comparison is facilitated by formulas for the locations of singularities close to the Fermi energy in the DOS for arbitrary (n,m) nanotubes.[45,46] Singularities in the DOS are expected to occur at energies

$$E_1 = \pm 3 d_{nn} \gamma_0 / d, \quad E_2 = 2 E_1 \quad \text{(conducting tubes)}, \tag{7}$$

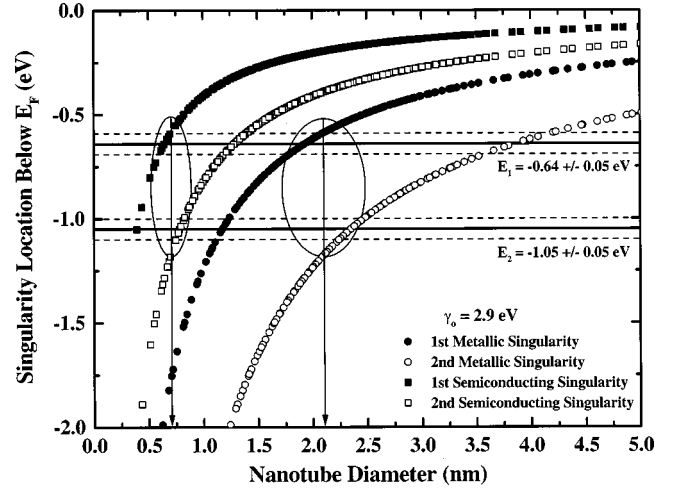$$E_1 = \pm d_{nn} \gamma_0 / d, \quad E_2 = 2 E_1 \quad \text{(semiconducting tubes)}. \tag{8}$$

FIG. 6. A comparison between the location of the two features labeled E_1 and E_2 (horizontal lines) measured from the field-emission total-energy distribution (TED) (see Fig. 5) with predictions for the location of singularities (obtained from Refs. 45 and 46) in the density of states (below E_F) for (n,m)SWNT's. The closed ($\bullet$) and open ($\circ$) circles represent the first and second singularities in the density of states for metallic nanotubes. The closed ($\blacksquare$) and open ($\square$) squares represent the first and second singularities for semiconducting nanotubes. The two regions which overlap with our experimental data are indicated by the ovals.

In Eqs. (7) and (8), d is the diameter of the nanotube and is given by

$$d = \sqrt{3} d_{nn} \sqrt{m^2 + mn + n^2} / \pi, \tag{9}$$

where d_{nn} is the C-C nearest bond distance (0.142 nm) and γ_0 is the $pp\pi$ hopping interaction. The best value of γ_0 is still under debate, so in the analysis below, we consider a range of values for this parameter ($\gamma_0 = 2.9 \pm 0.2$ eV).

Figure 6 compares the location of the two experimental features (at energies below E_F) with the location of the first two singularities (below E_F) in the DOS for both semiconducting and metallic nanotubes. When making this comparison, we assume the singularities in the DOS given in Eqs. (7) and (8) persist as the uncapped end in the nanotube is approached. This assumption is consistent with recent calculations presented by De Vita et al.[7] which suggest that the singularities soften into peaks (but do not disappear) at the uncapped end. At this time, we do not consider further modifications to the DOS, such as additional states which calculations show are created by defects,[47] or possible shifts in energy due to tube-tube interactions.

From Fig. 6, we conclude there are two likely diameters of nanotubes which are capable of providing agreement with the energies of both of the two experimental features measured (see two regions enclosed by ellipses). One region contains metallic nanotubes with diameters of ~ 2.1 nm, the other contains semiconducting nanotubes with diameters near ~ 0.7 nm. The range of (n,m) values for those nanotubes having DOS singularities falling within the two regions ($E_1 = -0.64 \pm 0.05$ eV and $E_2 = -1.05 \pm 0.05$ eV) are shown as shaded regions in Fig. 7. The metallic nanotubes are indicated by the region marked **M**, and the semiconducting nanotubes fall within the region marked **S**. We conclude that
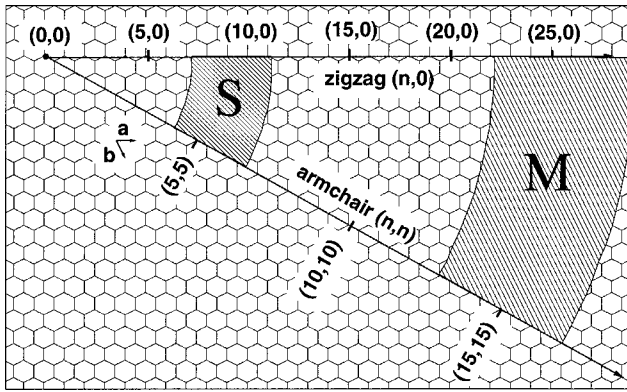
FIG. 7. A tabulation of the (n,m) values for nanotubes that have singularities in the density of states roughly corresponding to the features measured in the field-emission energy distributions. The shaded region marked **M** indicates the range of (n,m) for metallic nanotubes that have at least one singularity in the DOS that matches our experimental data. **M** indicates that only metallic nanotubes in this shaded region are to be considered. The shaded region marked **S** indicates the range of (n,m) for semiconducting nanotubes that have at least one singularity in the DOS that matches the experimental data. **S** indicates that only semiconducting nanotubes in this shaded region are to be considered. The extent of the shaded regions include an estimated uncertainty in the value of $\gamma_0 = 2.9 \pm 0.2$ eV.

at this time, it is not possible to uniquely identify the (n,m) value for the emitting nanotube based on the position of the two features alone.

C. Field-ion microscopy of a SWNT rope

FIM is an ideal tool to augment field-emission studies because of its inherent high magnification, thus allowing the possibility of imaging individual atoms at the end of the nanotube. However, *a priori*, the detailed geometric end form of the SWNT rope is not known, leading to some ambiguity in what form FIM images might take. To better understand the FIM process from a rope of SWNT's, various models of the rope's end form were considered. These models included (i) model *A*, a rope with one SWNT protruding further than others, (ii) model *B*, a rope with all of its SWNT's terminated evenly, and (iii) model *C*, a rope having a smoothly rounded end. In all of these models, we assumed that the individual nanotubes were uncapped.

The same SWNT rope producing the electron emission discussed above was imaged in the FIM using both Ar and He as the imaging gas. Carbon atoms in graphite require an electric field of 1433 MV/cm to be field evaporated from the surface;[48] however Rinzler *et al.* reported the "unraveling" of MWNT's at much lower field strengths.[26] For this reason, the first images were taken using Ar to reduce the possibility of the rope breaking apart in the high electric field. The rope was first imaged using Ar at ~1 kV, which corresponds to an applied electric field of ~2 MV/cm. These argon-ion FIM images were weak and showed little detailed atomic structure. We then switched to He to take advantage of its higher resolution and higher best image field, resulting in brighter images.

Initially, the FIM images consisted of a few random spots distributed across the screen. With time, the image changed
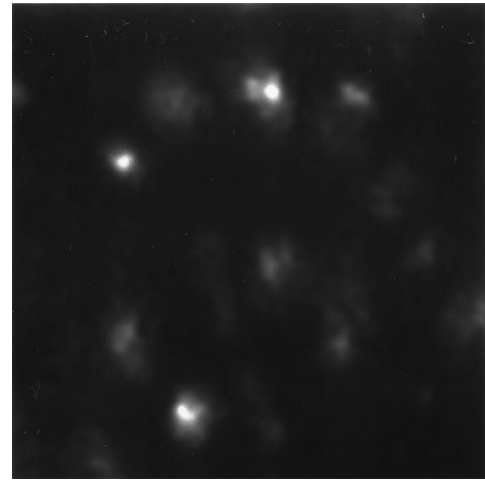

FIG. 8. A He field-ion microscope (FIM) image obtained from a SWNT rope. This image was taken at ~100 K, with the SWNT rope biased at 5700 V with respect to the ground.

and eventually a number of reasonably stable ring structures appeared across the viewing area. A cropped image of one of these ringlike structures is shown in Fig. 8. The observed ring structure consists of nine features located around the circumference of a circle with an additional two or three faint features located inside the ring's circumference. These features are shown more clearly by a contour plot made from the digitized FIM image [see Fig. 9(a)]. Analysis of the angular separation of these spots reveal they are separated from each other by an angle of ~28°, as indicated by the radial grid superimposed on the contour plot in Fig. 9(a). This indicates that the perimeter of the nanotube is comprised of $360°/28° \simeq 13$ such features, suggesting the nanotube is of $(13,m)$ or $(n,13)$ variety. This conclusion is consistent with a (19, 13) nanotube which is located within the region marked **M** in Fig. 7 above.

In FIM, the location of spots is related to the position of atoms protruding from the end form of the SWNT rope. We use a thin-shell model for simulating FIM images[48–50] to allow a better comparison between experiment and structural expectations. The length of C-C bonds in graphite is 0.14 nm. It is reasonable to assume that this is also true in carbon nanotubes.[3,10] The resolution of the FIM is roughly 0.25 nm, under the best of conditions, i.e., He imaging of a carefully field evaporated tip at 4 K. The image in Fig. 8 was taken using He as an imaging gas at 100 K; therefore, the resolution is not optimal. These considerations were incorporated into the thin-shell model (see Sec. II B) by convoluting the simulated image spots with a Gaussian to mimic the finite resolution.

The observed ring structure in Fig. 8 is consistent with model *A* mentioned earlier, that is, one SWNT which protrudes further above the rope's end. Using the projection model discussed in Sec. II B, it is possible to simulate expected FIM images from nanotubes. In what follows, we stay with the assumption that the end cap of the nanotube contributing to the field-ion image has been removed during the cutoff process (i.e., while mounting). The assumption of a missing end cap is entirely consistent with our FIM observations. It is likely that the end of the rope was further eroded by a field evaporation process during the FIM experiment.
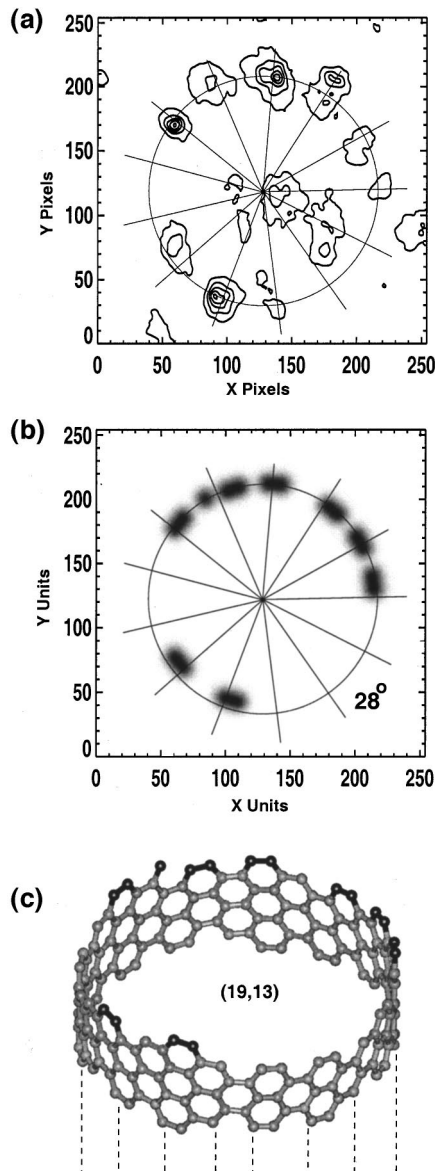
(a)

(b)

(c)

(19,13)

FIG. 9. (a) A contour plot from the digitized FIM image of a SWNT shown in Fig. 8. The solid radial lines are fiducial markers, and are spaced by 28°. In (b), a calculated FIM image from a (19, 13) nanotube. In (c), a schematic diagram of the nanotube used to produce the simulated FIM image in (b). The atoms imaged in the FIM simulation are shaded.

We note, in passing, that even a nanotube with an end cap, once eroded, may stay open due to chemisorbed He introduced during the field-ion measurement. For instance, it has been reported that high electric fields, such as the ones encountered in FIM, cause significant polarization of He atoms,[51,52] resulting in field-induced chemical adsorption of He onto kink sites and atomic planes on FIM tips. The presence of such polarized He atoms may be sufficient to hold the end of the nanotubes open, rather than allowing them to close and form hemispherical end caps.

To learn more about the atomic structure of carbon nanotube end forms, we simulated field-ion images from a variety of nanotubes. Our simulations show that (n,n) and $(n,0)$ nanotubes produce highly symmetric ring patterns with field-ion features located evenly around a circle. This symmetry

does not match the spots observed in our experimental data. Nanotubes of the (n,m) variety are more likely to give end forms with missing atoms, providing an explanation for the missing features observed around the ring's circumference in Fig. 9(a).

In trying to fit the experimental FIM image, there is some flexibility in the exact choice of n and m, although the angular position of the spots observed experimentally clearly provides restrictions on the range of n and m. In addition, we have limiting values for n and m suggested from our field-emission TED's. To illustrate the simulation technique, we show a calculated FIM image from a (19, 13) SWNT in Fig. 9(b). The geometry of the tube structure is given in Fig. 9(c). Although this agreement is encouraging and consistent with the conclusions drawn from the field-emission work, it is probably not unique. More work is required to make a more positive identification from the FIM images alone.

Using rough estimates for the magnification of our FIM, we can demonstrate that the ring structure in Fig. 8 is indeed consistent with the diameter expected for a SWNT. As discussed above, it is likely that the rope imaged has an uneven end, i.e., one SWNT protrudes furthest above the end of the rope. The electric-field lines around this one SWNT will diverge more rapidly than those from the entire rope, enhancing the local magnification. The precise magnification will therefore depend upon how far the one SWNT protrudes above its nearby neighbors. However, rough limits on the magnification can be set.

Assuming a typical value of 1.5 for α in Eq. (1), a lower limit for the magnification of our FIM is $\sim 1.0 \times 10^7$, assuming the entire rope (i.e., a radius of ~ 8.5 nm) controls the magnification. If instead, the radius of a SWNT (i.e., a radius of ~ 1.1 nm) is inserted into Eq. 1, an upper limit for the magnification of 8×10^7 is obtained. The average radius of the ring structure shown in Fig. 8, was found to be 1.4 cm on the multichannel plate, implying a magnification of 2×10^7. This result is closer to the magnification expected if the diameter of the SWNT rope controls the field enhancement.

IV. CONCLUSIONS

An individual 17-nm-diam rope comprised of ~ 70 single-walled carbon nanotubes (SWNT's) was mounted and studied using transmission electron microscopy, field emission, and field-ion microscopy techniques under UHV conditions. The electron emission pattern from the rope was recorded and found to exhibit electron emission over a half-angle of $\sim 7°$. No unusual striations were observed in the pattern. The dependence of the emitted current as a function of applied voltage was studied and found to obey a Fowler-Nordheim equation, indicating that electron emission is due to a field emission process from a surface having a work function $\phi \approx 5.1$ eV. Using estimates of the rope diameter obtained from complementary TEM studies, an estimate of the field enhancement around the apex of the SWNT rope was obtained. This value is roughly ten times greater than that normally obtained from a standard W field emitter tip and is entirely consistent with the sharp end form expected for a SWNT rope.

A measurement of the total energy distribution (TED) of field-emitted electrons was also performed. Using the field

enhancement factor from the Fowler-Nordheim analysis, the applied electric field was estimated and used to fit the measured total-energy distribution to a free-electron model. The resulting fits showed reasonable overall agreement to theoretical expectations, and provided further evidence that the SWNT rope had electrical properties which were metallic in nature. The FWHM of the emitted electron distribution was measured to be 0.35 ± 0.05 eV in an electric field of $F = 6 \times 10^7$ V/cm. This value includes the (estimated) 0.20-eV FWHM resolution of the energy analyzer. Distinct features were present on the trailing edge of the energy distribution, and were located at energies of 0.64 ± 0.05 eV and 1.05 ± 0.05 eV below the Fermi energy. We attribute these features to electron emission from singularities in the electronic density of states that are characteristic of one-dimensional nanotubes. By comparing the location of these singularities to theoretical calculations, a range of (n,m) values were found to be consistent with our experimental data.

Field-ion images of the same SWNT rope showed evidence that a single nanotube was protruding from the rope, producing a circular field-ion image. Simulations of a FIM image from a single (19, 13) nanotube were found to roughly match the experimental field-ion image.

This study sketches out a strategy that may be useful in the future characterization of electron emission sources constructed from nanotubes. By measuring field-emission energy distributions followed by a field-ion microscopy study, it seems possible to determine both the electronic and structural properties of individual nanotubes.

[1] J. W. Mintmire, B. I. Dunlap, and C. T. White, Phys. Rev. Lett. **1992**, 631 (1992).

[2] K. Tanaka, K. Okahara, M. Okada, and T. Yamabe, Chem. Phys. Lett. **191**, 469 (1992).

[3] M. S. Dresselhaus, G. Dresselhaus, and P. C. Eklund, *Science of Fullerenes and Carbon Nanotubes* (Academic Press, New York, 1996).

[4] V. Meunier and Ph. Lambin, Phys. Rev. Lett. **81**, 5588 (1998).

[5] R. Tamura and M. Tsukada, Phys. Rev. B **52**, 6015 (1995).

[6] D. L. Carroll, P. Redlich, P. M. Ajayan, J. C. Charlier, X. Blase, A. De Vita, and R. Car, Phys. Rev. Lett. **78**, 2811 (1997).

[7] A. De Vita, J. C. Charlier, X. Blase, and R. Car, Appl. Phys. A: Solids Surf. **68**, 283 (1999).

[8] S. Iijima, Nature (London) **354**, 56 (1991).

[9] T. W. Ebbesen and P. M. Ajayan, Nature (London) **358**, 220 (1992).

[10] B. I. Yakobson and R. E. Smalley, Am. Sci. **85**, 324 (1997).

[11] Z. Zhang and C. M. Lieber, Appl. Phys. Lett. **62**, 2792 (1993).

[12] N. Lin, J. Ding, S. Yang, and N. Cue, Carbon **34**, 1295 (1996).

[13] H. Dai, E. Wong, and C. Lieber, Science **272**, 523 (1996).

[14] Jeroen W. G. Wildöer, L. C. Venema, A. G. Rinzler, R. E. Smalley, and C. Dekker, Nature (London) **391**, 59 (1998).

[15] T. W. Odom, J. L. Huang, P. Kim, and C. M. Lieber, Nature (London) **391**, 62 (1998).

[16] P. Kim, T. W. Odom, J-L. Huang, and C. M. Lieber, Phys. Rev. Lett. **82**, 1225 (1999).

[17] T. W. Ebbesen, H. J. Lezec, H. Hiura, J. W. Bennett, H. F. Ghaemi, and T. Thio, Nature (London) **382**, 54 (1996).

[18] B. H. Fishbine, C. J. Miglionico, K. E. Hackett, K. J. Hendricks, X. K. Wang, R. P. H. Chang, J. D. Shovlin, and M. E. Kordesch, in *Science and Technology of Fullerene Materials*, edited by P. Bernier, T. U. Ebbesen, D. S. Bethune, R. M. Metiger, L. Y. Chiang, and J. W. Mintmir, MRS Symposia Proceedings No. 359 (Materials Research Society, Pittsburgh, PA, 1995), p. 9.

[19] M. A. More and D. S. Joag, J. Phys. D **25**, 1844 (1992).

[20] Yu. V. Gulyaev, Z. Ya. Kosakovskaya, N. I. Sinitsyn, G. V. Torgashov, E. A. Fedorov, Yu. F. Zakharchenko, and V. P. Val'chuk, in *Science and Technology of Fullerene Materials* (Ref. 18), p. 99.

[21] M. S. Mousa, Appl. Surf. Sci. **94/95**, 129 (1996).

[22] B. H. Fishbine, C. J. Miglionico, K. E. Hackett, and K. J. Hendricks, in *Novel Forms of Carbon II*, edited by C. L. Renschler, D. M. Cox, J. J. Pouch, and Y. Achiba, MRS Symposia Proceedings No. 349 (Materials Research Society, Pittsburgh, PA, 1994) p. 319.

[23] Q. H. Wang, T. D. Corrigan, J. Y. Dai, R. P. H. Chang, and A. R. Krauss, Appl. Phys. Lett. **70**, 3308 (1997).

[24] J.-M. Bonard, T. Stora, J.-P. Salvetat, F. Maier, T. Stöckli, C. Duschl, L. Forró, W. A. de Heer, and A. Châtelain, Adv. Mater. **9**, 827 (1997).

[25] W. A. de Heer, J.-M. Bonard, K. Fauth, A. Châtelain, L. Forró, and D. Ugarte, Adv. Mater. **9**, 87 (1997).

[26] A. G. Rinzler, J. H. Hafner, P. Nikolaev, L. Lou, S. G. Kim, D. Tománek, P. Nordlander, D. T. Colbert, and R. E. Smalley, Science **269**, 1550 (1995).

[27] J.-M. Bonard, F. Maier, T. Stöckli, A. Châtelain, W. A. de Heer, J.-P. Salvetat, and L. Forró, Ultramicroscopy **73**, 7 (1997).

[28] J.-M. Bonard, J.-P. Salvetat, T. Stöckli, W. A. de Heer, L. Forró, and A. Châtelain, Appl. Phys. Lett. **73**, 918 (1998).

[29] J. M. Cowley, P. Nikolaev, A. Thess, and R. E. Smalley, Chem. Phys. Lett. **265**, 379 (1997).

[30] A. M. Rao, E. Richter, S. Bandow, B. Chase, P. C. Eklund, K. A. Williams, S. Fang, K. R. Subbaswamy, M. Menon, A. Thess, R. E. Smalley, G. Dresselhaus, and M. S. Dresselhaus, Science **275**, 187 (1997).

[31] H. Dai, J. H. Hafner, A. G. Rinzler, D. T. Colbert, and R. E. Smalley, Nature (London) **384**, 147 (1996).

[32] P. M. Ajayan, T. W. Ebbesen, T. Ichihashi, S. Iijima, K. Tanigaki, and H. Hiura, Nature (London) **362**, 522 (1993).

[33] S. H. Tsai, C. W. Chao, C. L. Lee, and H. C. Shih, Appl. Phys. Lett. **74**, 3462 (1999).

[34] T. T. Tsong, *Atom Probe Field Ion Microscopy* (Cambridge University Press, New York, 1990).

[35] R. Gomer, *Field Emission and Field Ionization* (Harvard University Press, Cambridge, MA, 1961).

[36] D. Lovall, M. Buss, R. P. Andres, and R. Reifenberger, Phys. Rev. B **58**, 15 889 (1998).

[37] T. Castro, R. Reifenberger, E. Choi, and R. P. Andres, Surf. Sci. **234**, 43 (1990).

[38] R. Gomer, J. Chem. Phys. **28**, 457 (1958).

[39] K. A. Dean and B. R. Chalamala, J. Appl. Phys. **85**, 3832 (1999).

[40] R. H. Fowler and L. W. Nordheim, Proc. R. Soc. London, Ser. A **119**, 173 (1928).

[41] J. Hölzl and F. K. Schulte, *Work Function of Metals*, edited by G. Hohler, Springer Tracts in Modern Physics Vol. 85 (Springer-Verlag, Berlin, 1979).

[42] R. D. Young, Phys. Rev. **113**, 110 (1958).

[43] J. W. Gadzuk and E. W. Plummer, Rev. Mod. Phys. **43**, 487 (1973).

[44] R. Reifenberger, H. A. Goldberg, and M. J. G. Lee, Surf. Sci. **83**, 599 (1979).

[45] J. C. Charlier and Ph. Lambin, Phys. Rev. B **57**, R15 037 (1998).

[46] C. T. White and J. W. Mintmire, Nature (London) **394**, 29 (1998).

[47] M. P. Anantram, J. Han, and T. R. Govindan, in *Molecular Electronics: Science and Technology*, edited by A. Aviram and M. Ratner (New York Academy of Sciences, New York, 1998), Vol. 852.

[48] E. W. Müller and T. T. Tsong, *Field Ion Microscopy, Principles and Applications* (American Elsevier, New York, 1969).

[49] A. J. W. Moore, J. Phys. Chem. Solids **23**, 907 (1962).

[50] M. K. Miller and G. D. W. Smith, *Atom Probe Microanalysis* (Materials Research Society, Pittsburgh, PA, 1989).

[51] H. J. Kreuzer, Surf. Sci. **246**, 336 (1990).

[52] W. A. Schmidt, Yu. Suchorski, and J. H. Block, Surf. Sci. **301**, 52 (1994).